High-performance and sustainable aerosol filters based on hierarchical and crosslinked nanofoams of cellulose nanofibers

Ukkola, Jonne

2021-08-10

High-performance and sustainable aerosol filters based on hierarchical and crosslinked nanofoams of cellulose nanofibers

Jonne Ukkola [a], Markus Lampimäki [b], Ossi Laitinen [a], Tomi Vainio [b], Juha Kangasluoma [b], Erkki Siivola [b], Tuukka Petäjä [b], Henrikki Liimatainen [a,*]

[a] *Fibre and Particle Engineering Research Unit, University of Oulu, P.O. Box 4300, FI-90014 Oulu, Finland*
[b] *Institute for Atmospheric and Earth System Research (INAR), University of Helsinki, FI-00014 Helsinki, Finland*

ARTICLE INFO

ABSTRACT

Nano-structured and porous foams derived from crosslinked cellulose nanofibers (CNF) were designed and tailored as highly efficient aerosol filters. The lignin-containing CNF was prepared from a recycled milk-container board using deep eutectic solvent pretreatment and mechanical grinding. The nanofoams or aero-gels were formed in different densities (initial CNF concentration of 0.2–1.0 wt%) with a freeze-drying process using two silane compounds for strengthening the structure. The filtration performance of nanofoams was studied with a Differential Mobility Particle Sizer (DMPS) setup using 10–500 nm NaCl aerosol particles. DMPS determines particle number size distribution of particles passing through nanofoams which is used to calculate the filtration performance. All nanofoams, which possessed porosity from 99.1% to 99.8% and specific surface area from 5.9 $m^2\,g^{-1}$ to 18.6 $m^2\,g^{-1}$, achieved good filtration performance (>96%) in the measured particle size range. Very high filtration efficiency (>99.5%) was achieved with the 0.7 wt% nanofoam sample for particles smaller than 360 nm. Based on the quality factors (QF), 0.3 wt% nanofoam produced the lowest pressure drop yet with relatively high filtration efficiency and resulted in the highest QF value that met the N95 standard requirements of respirator face masks. The structure and thickness of the nanofoam filter makes possible high particle bearing without loss on its performance.

1. Introduction

Air pollution and various aerosols are one of the major concerns that pose threat to health and climate. Airborne particulate matter (PM) pollution in the atmosphere causes serious environmental challenges and threats to human health, along with other pollutants such as chemical vapors, bacteria and viruses (Davidson et al., 2005; Kim et al., 2015; Souzandeh et al., 2019; Maciej et al., 2012). The source of PM is either natural or human caused. Anthropogenic sources include coal, fossil fuel, biomass burning, and industrial and agricultural activities (Davidson et al., 2005; Kim et al., 2015). Respiratory symptoms are the major concern of the PM pollution as it causes direct damage to the lungs and the respiratory system and, through them, to the cardiovascular system leading to premature deaths (Kim et al., 2015; Shah et al., 2013). In most studies, PM with aerodynamic diameter smaller than 2.5 μm (PM2.5) has been reported to have a serious impact on respiratory health, since it penetrates with ease into human lungs and the respiratory system (Lu et al., 2018; Maciej et al., 2012). Therefore, the cleaning of polluted air is becoming increasingly important. In addition, the use of high-level aerosol filtering materials has become gradually more important in the global medical field because of pathogens spreading through airborne transmission. For instance, only respirators (N95 or N99 by US standards and FFP2 or FFP3 by European standards) can provide effective protection against airborne viruses, and those are currently recommended to be worn during aerosol-generating medical procedures (e.g., intubation) on patients with SARS Co–V infection, avian influenza, and pandemic influenza in major parts of the world ("A new material for airborne virus filtration," 2011; Siegel et al., 2007).

Numerous studies have paid attention to the development of filters for nano- and micro-particles from air (Qiao et al., 2020; Souzandeh et al., 2019). Previously employed nanofiber filter materials include polymer-based electrospun fibers (Subbiah et al., 2005) generated from nylon, polycarbonate, polyurethane, and polyethylene oxide (Ahn et al., 2006; Tsai et al., 2002). Despite the filters' good filtering properties,

* Corresponding author.
  E-mail address: henrikki.liimatainen@oulu.fi (H. Liimatainen).

fabrication of those filters require chemical agents and unrenewable raw materials, and they are generally nonbiodegradable (Lu et al., 2018; Macfarlane et al., 2012; Podgórski et al., 2006). A widely recognized sustainable alternative for petroleum-based chemicals and materials is cellulose, which is a green, biodegradable and recyclable polymer (Nechyporchuk et al., 2016). However, morphology and surface smoothness of native cellulose fibers limit their use and efficiency in small-particle filtrating applications (Macfarlane et al., 2012). Therefore, utilization of fibrillated cellulose and nanocellulose have been shown to effectively increase the filtration performance of cellulose-based air filters (Lu et al., 2018; Macfarlane et al., 2012).

Recently, many studies related to effective filter materials based on aerogels or foams have been published (Kim et al, 2016, 2017; Ma et al., 2019; Wang et al., 2019; Zhang et al., 2019). Aerogels can be divided into polymer aerogels (Deuber et al., 2018; Mader et al., 2018; Qian et al., 2018; Zhai and Jana, 2017), carbon-based aerogels (Huber et al., 2017; Wu et al., 2017), and biomass-based aerogels (Deuber et al., 2018; Fan et al., 2017). Furthermore, nanofoams or aerogels based on cellulose nanofibers (CNFs) have gained increasing scientific attention due to desired mechanical properties, low density, high porosity, chemical versatility, and natural biodegradability (Karzar Jeddi et al., 2019; Korhonen et al., 2011; Laitinen et al., 2017; Zanini et al., 2017; Zeng et al., 2019). Aerogels are a class of highly porous solid materials prepared from wet gels by drying while the solids maintain mainly their wet-state structure (Innerlohinger et al., 2006; Zhang et al., 2019). Because of their versatile properties, nanocellulose aerogels have been studied in a variety of applications such as oil sorption (Jiang and Hsieh, 2014; Karzar Jeddi et al., 2019; Laitinen et al., 2017), biomedical materials (Lu et al., 2014), nanocomposites (Nissilä et al., 2019), and thermal insulation (Wang et al., 2020). Nanofoams' inherent properties such as high surface area and very high porosity are advantageous properties also for air filtration applications (Barhate and Ramakrishna, 2007; Ma et al., 2019; Sehaqui et al., 2010; Wang et al., 2019; Zeng et al., 2019; Zhang et al., 2019). Previously, CNFs and fibrillated cellulose have been utilized to prepare aerogels for filtration of airborne particles (Alexandrescu et al., 2016; Lu et al., 2018; Ma et al., 2018; Macfarlane et al., 2012) and to improve the filtration properties of commercially available high-efficiency particulate filters (HEPA) (Kim et al, 2016, 2017; Nemoto et al, 2015, 2016).

In the current world situation, there is an emerging and continuous need for new types of high-efficient and cost-effective filtration materials derived from sustainable and easily available sources such as recycled fiber materials. Moreover, aerogels prepared by freeze drying have demonstrated extremely low density and high porosity, which result in a lower pressure drop during the filtration process (Zeng et al., 2019; Zhang et al., 2018). In this study, we present the preparation of cost-effective (Laitinen et al., 2017) and environmentally friendly lignin-containing CNF nanofoams from recycled waste material to be used as highly efficient aerosol filters. CNF nanofoams were prepared from deep eutectic solvent (DES)-pretreated and nanofibrillated recycled milk-container board (MCB) through a simple freeze-drying procedure and modified for hydrophobicity and reinforced structure by silylation agents. The aerosol filtration efficiency of the obtained crosslinked highly porous and low-density nanofoams was studied using a Differential Mobility Particle Sizer (DMPS) setup reaching satisfactory performance even for the smallest nanoparticles. DMPS is a widely used system in atmospheric aerosol research to measure particle number size distributions in the submicrometer diameter range (Wiedensohler et al., 2012). DMPS covers particle diameter ranges from 3 to 800 nm and the particle diameter and particle number size distribution of the aerosol are focal parameters when effects of the aerosol particles to human health and climate are studied (Kulmala et al., 2012; Wiedensohler et al., 2012). In our study, DMPS proved to be valuable and reliable equipment to determine the aerosol filtration properties of lignin-containing CNF nanofoams and it could also be adapted to measure other filtration materials.

2. Materials and Methods

2.1. Materials

A recycled milk-container board (MCB) was collected directly from refuse collections and used as cellulose raw material. The MCB was pulped without chemicals using a Kenwood KM020 pulper (UK), which has an operating principle similar to the Hobart pulper. The pulping was conducted for 10 min using a rotor speed of 2 (~250 rpm) at a consistency of 15% at approximately 45 °C. The cellulose pulp was then washed and screened using a Somerville screen (Lorentzen & Wettre; Sweden). Urea (97%) and choline chloride (>98%) were purchased from Borealis (Austria) and Algry Qu Mica (Spain), respectively. Methyltrimethoxysilane (98%, MTMS) was obtained from Evonik Industries (Germany), and hexadecyltrimethoxysilane (>85%, HDTMS) was from Sigma-Aldrich (Germany). All chemicals were used as received, without further purification.

2.2. DES pretreatment and nanofibrillation of MCB

After pulping, four batches of MCB were pretreated in DES solution that was produced by oven heating 1620 g of choline chloride and 1223 g of urea in a 5 L beaker at 100 °C until the mixture liquefied, after which it was placed into a water bath at 100 °C under constant stirring for approximately 5 min to obtain a clear and colorless liquid. Next, 25 g (abs) of MCB was added at a consistency of ~30 wt% to the DES solution and mixed for 120 min, after which the beaker was removed from the water bath, and 1000 mL of deionized water was added while stirring. The DES treated lignin-containing cellulose was washed with water using a Somerville screen until clear wash water was obtained.

The washed MCB was nanofibrillated using a Masuko super mass-colloider grinder MKCA6-2 J (Japan) to produce cellulose nanofibers (MCB CNFs). First, the stones of the grinder were carefully brought into close contact, which was verified by a low friction sound. Then aqueous MCB suspension (consistency 1.5%) passed two times through the grinder using a zero grinding gap between the stones, after which the stones were adjusted to negative grinding values. The gap values of −20, −40, −50, −70, and −80 μm were used for 10 passages. Characterization of obtained lignin-containing CNF and MCB suspension is briefly described below.

Fig. 1 shows the rotational viscosity (based on Brookfield DV-II + Pro EXTRA (USA) rotational viscometer) of the MCB hydrogel after its 10th pass through the Masuko grinder at a consistency of 0.5%. Rotational viscosity also indicates the degree of polymerization of the cellulose. The
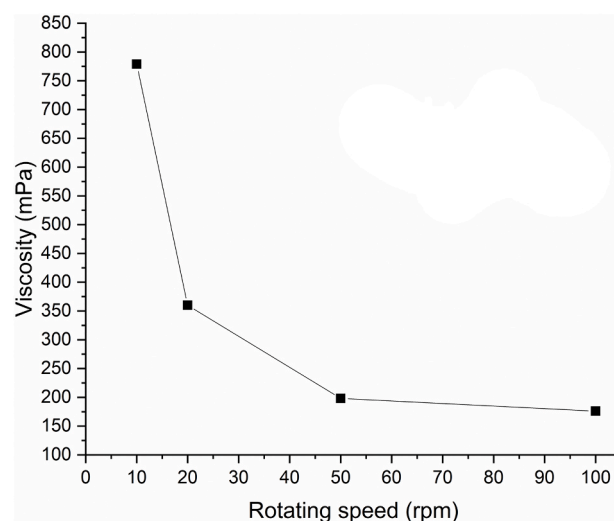

Fig. 1. Rotational viscosity of lignin-containing CNF suspension.

visual appearance (based on TEM imaging, A Tecnai G2 Spirit (The Netherlands)) of the CNFs from MCB pulp shows the individual particles having diameter in the range of 2–80 nm (Suopajärvi et al., 2017). The yield of the nanofibrillation procedure was almost 100% due to the combined Masuko grinding method and the used DES chemistry (the mixture of choline chloride–urea). The crystallinity index (based on wide-angle X-ray diffractometry (WAXD) using a Siemens D5000 diffractometer (USA)) of the CNFs after 10th passes through the Masuko grinder was 53.5%. The charge of the MCB pulp (-0.10 mmol/g) was analyzed via conductometric titration using a procedure described by (Rattaz et al., 2011) and (Katz et al., 1984). The lignin content (12.3%) of the MCB was determined using TAPPI-T 222 om-02 standard.

2.3. Preparation of the crosslinked nanofoam filters

Nanofoams were prepared using a fast freezing and vacuum drying method according to Laitinen et al. (2017) with slight modifications. Shortly, MCB CNF suspensions were diluted with deionized water to various consistencies (Table 1) to obtain nanofoams with different porosities and densities. Diluted suspensions were then homogenized using an Ultra-Turrax mixer at 10,000 rpm for 30 s, and pH of suspension was adjusted to 4 with 0.5 M HCl. Two silylation agents (MTMS and HDTMS) were used together at the ratio of 1:1 to both crosslink CNFs and to enhance the hydrophobicity of the nanofoams. Two silane solutions were prepared separately by diluting silanes (MTMS and HDTMS) in ethanol at 20 wt% and mixed using a magnetic stirrer for 10 min. Then, a certain amount of both freshly prepared silane solutions were added by micropipette into each diluted CNF suspension at a ratio of 1:8 relative to the CNF amounts and let to react for 120 min at room temperature.

Next, silylated lignin-containing CNF suspensions were cast in round aluminum molds (height of 35 mm and inside diameter of 20–22 mm, depending on the consistency-related drying shrinkage), frozen quickly in liquid nitrogen and then moved to a Scanvac Coolsafe 55–15 Pro (Denmark) freeze-dryer (-54 °C, 0.05 mbar) for 72 h to obtain CNF nanofoams. The nanofoams were let to cure in oven at 40 °C overnight before the next step.

The nanofoams were carefully mounted through a customized copper reducer into a copper bush ring (inside diameter: 20 mm, height: 12 mm) and cut to a proper height using a surgical blade to be inserted in the DMPS filtration setup. The diameter of each nanofoam was approximately 0.5–1 mm larger than the diameter of the bush ring to ensure tight fitting to the ring and to prevent particle leakage during the filtration experiments. Final sealing was done using acrylate glue. The preparation principle of crosslinked nanofoams is presented in the Fig. 2.

2.4. Characterization of nanofoam filters

Field emission scanning electron microscopy (FESEM, Zeiss Ultra Plus, Germany) was used for imaging the nanofoams with an acceleration voltage of 5 kV and a working distance of approximately 5 mm. The specimens were obtained by cleaving the nanofoams to expose cross-sectional areas, attaching them to a sample holder with a carbon tape and then sputter coating them with a thin platinum layer.

The Brunauer–Emmett–Teller (BET) specific surface area of the nanofoams was determined using an ASAP 2020 system (Micromeritics,

USA) by N_2 physisorption at -196 °C. The samples were prepared by tearing small pieces from nanofoams using a pair of forceps, carefully moving to a long-necked analysis flask, and then oven drying at 105 °C overnight before the analysis.

The porosity (P, %) of the nanofoams was calculated as

$$P_{nanofoam} = \left(1 - \frac{\rho_{nanofoam}}{\rho_f}\right) * 100\% \tag{1}$$

where $\rho_{nanofoam}$ is the apparent density of the nanofoam and ρ_f is the density of the bulk cellulose (1.528 g cm^{-3}). The apparent densities of the nanofoams (ρ, g cm^{-3}) were calculated using the formula

$$\rho_{nanofoam} = \frac{m}{V} \tag{2}$$

where m (g) is the mass, and V (cm^3) is the volume of the nanofoam as measured by a digital caliper.

2.5. DMPS aerosol filtration setup

The aerosol generator and used filtration measurement setup are illustrated in Fig. 3. An atomizer aerosol generator (TOPAS ATM 221) was employed to generate sodium chloride (NaCl) aerosol particles from 5 wt% solution prepared in Millipore water. NaCl droplets were dried by a silica dryer (TOPAS) and charged using a Am bipolar diffusion charger. Am bipolar diffusion charger consist of a cylindrical metal holder in which 241Am foil is placed in the outer wall of the cylinder. The gas inlet and outlet are at the top and bottom of the cylinder, through which the aerosol sample enters and exits the charger. The charger creates bipolar ion cloud that brings the sample particles into a known steady state charge distribution (Wiedensohler, 1988).

An exhaust for overflow with the HEPA-filter was used after the nebulizer to avoid any overpressure to build into the setup. The valve in the exhaust allowed fine-tuning of the NaCl aerosol flow to the Differential Mobility Analyzer (DMA). Primary NaCl particle concentration of 8000–10,000 cm^{-3} was obtained. The NaCl aerosols generated by the atomizer possess well known particle size distribution from 10 nm to several hundred nanometers, which is well-adjustable and suitable for filter testing as reported by Topas ATM 221 Instruction Manual. The properties of NaCl particles have also been reported and documented in the standard SFS-EN 149: "Respiratory protective devices. Filtering half masks to protect against particles. Requirements, testing, marking". The concentration of NaCl and their particle size depend on the original salt solution concentration (this is presented in the original Instruction Manual as a Table). The TEM images of salt aerosols have been previously reported in Park et al. (2009). The particle number size distribution was classified by their electrical mobility with the Vienna-type Mobility particle sizer spectrometer with a classification length of 50 cm. A linear ramp of the DMA voltage corresponding to particle diameter ranging from 10 nm to 500 nm was produced using the LabView controlled 12.5 kV HV source (Fug HCN 7E-12500). Sheath flows in and out were monitored by mass flow meters (TSI 4000). Sample flow was frequently measured and adjusted using a primary flow meter (Bios Drycal DC-Lite). Sample flow rate to sheath flow rate of 1:10 was used with 20 L min^{-1} for the sheath and 2 L min^{-1} for the sample. The total concentrations of NaCl particles were measured by two identical Airmodus A20 Condensation Particle Counters (CPC's), both connected to the laboratory vacuum line and sampling 1 L min^{-1} via a critical orifice. One CPC was sampling in downstream from the sample and the other one prior to the sample for the reference concentration. The cutoff size for the CPCs is around 7 nm with the current settings ("A20 Condensation Particle Counter," n. d.).

Equal lengths of the conductive silicon tubing from the manifold were used for both CPCs. Prior to the filter measurement, the sample holder was characterized without the filter material to observe any losses (Fig. 4, left). The small difference in the NaCl concentrations

Table 1
Densities, porosities, and BET specific surface areas of the nanofoams.

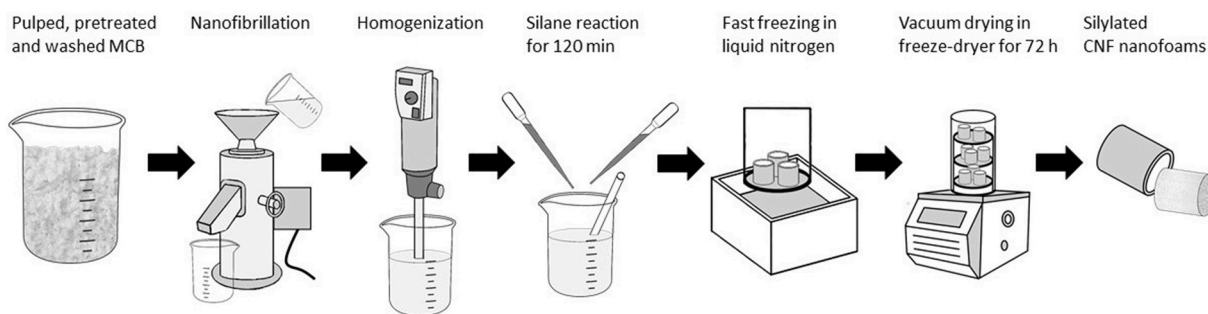| Sample name	Initial CNF concentration (wt %)	Density (g dm^{-3})	Porosity (%)	BET specific surface area (m^2 g^{-1})
MCB_1.0	1.0	13.9	99.1	5.9
MCB_0.75	0.75	10.5	99.3	11.1
MCB_0.5	0.5	10.4	99.3	11.0
MCB_0.3	0.3	4.4	99.7	15.4
MCB_0.2	0.2	2.8	99.8	18.6

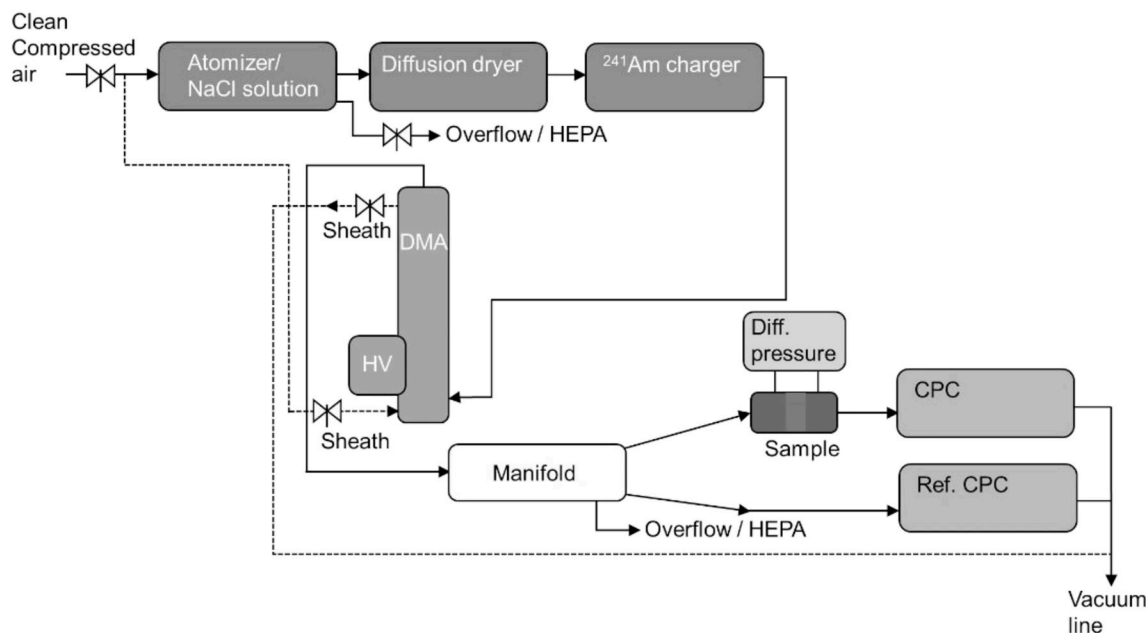**Fig. 2.** The preparation of crosslinked nanofoams of cellulose nanofibers.

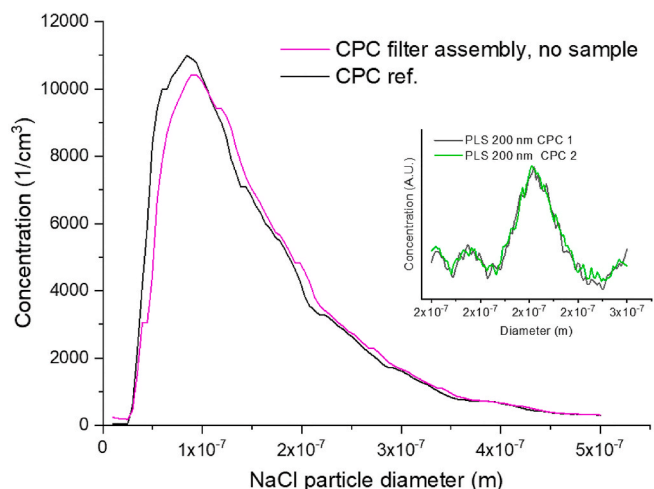**Fig. 3.** Aerosol filtration measurement setup.

Fig. 4. NaCl particle distribution measured without the filter sample (left). Reference polystyrene latex spheres (PLS) measured without the filter sample (right inset).

below 100 nm is likely due to losses induced by the filter assembly volume. Equal concentrations were observed for the 200 nm polystyrene latex spheres (PLS, TSI, Inc.) reference. Pressure drop, ΔP, over the filter

sample was measured by the differential pressure sensor (MPX5010DP K123AE).

In this study, each nanofoam filter sample was scanned three times, and averaged size distribution was then used for collection efficiency calculations. Since the measurements on each filter sample took a relatively short time (<15 min), no change in aerosol concentration or pressure difference due to deposited particles was observed. This so-called skin effect can have a significant role in submicron aerosol particle filtration in nanoscale fiber filters (Leung and Hung, 2012). Also, the particle flow from the atomizer remained stable during the measurements.

2.6. Aerosol filtration performance measurements of nanofoams

Only synthetic NaCl particles were used as a model aerosol in the current study in order to obtain well known, broad particle size range with high upstream concentration and thus good signal also from the downstream filter measurements. The synthetic NaCl particles enable to have a precise and well-controlled particle distribution, and to determine the filtration efficiency of the nanofoams as a function of aerosol size. Collection/filtration efficiency (E) was calculated for the particle size ranging from 10 nm to 500 nm from the CPC concentration ratio:

$$E \ [\%] = \left(1 - \frac{C_{filter}}{C_{ref}}\right)100 \tag{3}$$

The filter copper bush ring frame area and the corresponding filter sample diameter were selected to produce a constant face velocity of 5.3 cm s^{-1} with the 1 L min^{-1} flow to the CPC. Flows to CPCs were constrained by the critical orifice, and they remained stable throughout the measurements. Filter CPC's instrument pressure was also monitored to ensure a normal operating pressure range with each sample. A filter sample that is too thick or dense would cause underpressure inside the CPC and interfere with the measurements.

The filtration performance of the nanofoams was evaluated by calculating the Quality Factor (QF) (Macfarlane et al., 2012), which is defined as

$$QF = -\frac{\ln(1 - E)}{\Delta P} \tag{4}$$

where E is filter collection efficiency and ΔP is the pressure drop between upstream and downstream pressures. Larger values of QF indicate better filter quality, since high filtration efficiency with low pressure drop is a desired feature of filters.

3. Results and Discussion

3.1. Characterization of nanofoams

The cellulose nanofiber suspension from choline chloride–urea treatment and mechanical grinding had a yellowish color and a viscous gel-like visual appearance. It was observed that the fibrillation, viscosities (Fig. 1), and fiber distributions of the same raw material and concluded that the lignin-containing CNF contained both individual long nanofibers and larger nanofiber aggregates having diameter in the range of 2–80 nm.

In the freeze-drying process the crosslinked cellulose nanofibers were formed into a cylindrical, lightweight, highly porous, and sponge-like material. All these prepared nanofoams had visually a homogeneous structure without any visible discontinuities such as cracks or collapses in the structure. With lower consistencies (i.e., original CNF suspension concentration of 0.2 wt% and 0.3 wt%), the nanofoams were more difficult to handle during sample preparation because of their brittle character. The nanofoams from higher consistencies (up to 1.0 wt%) were stiffer and could be cut using a surgical blade. All nanofoams responded elastically to minor compression; however, transformations were readily nonreversible with the lower consistencies. In addition, minor shrinkage occurred in diameter direction during the drying process of nanofoams. Therefore, aluminum molds with diameters of 22 mm and 23 mm were used to ensure proper fitting of the nanofoams into copper bush rings (Fig. 5) without unnecessary compression.

The structural uniformity, porosity, and density of the nanofoam are directly related to the ratio of CNFs and water in the initial nanofiber suspension. At lower consistencies, the CNFs could not form mechanically strong porous networks (<1.0 wt%) because of low inter molecular hydrogen bonding (Jin et al., 2004; Sehaqui et al., 2010) and mechanical entanglement. Therefore, two silylation agents (MTMS and HDTMS) were used at the same time to promote the mechanical characteristics of nanofoams. It is well-known that MTMS is a crosslinking agent for cellulose (Zhang et al, 2014, 2015) that can chemically crosslink CNFs even at very low concentrations in aqueous conditions. HDTMS increases hydrophobicity of nanofoams because of its long carbon chain (Rafieian et al., 2018), and is not working as a crosslinking agent itself. On previous publication Laitinen et al. (2017) determined water contact angles (WCA) of similar silylated MCB nanofoams to be over 90° confirming hydrophobicity of the nanofoams. They have also noticed that if only MTMS is used the water contact angle is roughly 90–110°, while using both silylation agent at the same time water contact angle >150° can be achieved. In the same study (Laitinen et al., 2017) noticed the homogeneous silylation of the nanofoams was quantified using X-ray photoelectron spectroscopy (XPS) and the surface concentration of Si was determined to be 4.80 ± 0.76 at-%.

Table 1 shows densities, porosities, and BET specific surface areas of the nanofoams as functions of initial lignin-containing CNF suspension consistency. The decrease in nanofiber consistency from 1.0 wt% to 0.2 wt% brought the porosity of the nanofoams from 99.1% to 99.8% and the density from 13.9 g dm^{-3} to 2.8 g dm^{-3} while still maintaining the self-standing and firm structure of nanofoams. In addition, the specific surface area of the nanofoams increased with decreasing CNF concentration as also reported in the previous studies (Aulin et al., 2010; Sehaqui et al., 2010). The highest specific surface area was achieved with MCB_0.2 (18.6 m^2 g^{-1}), and the lowest with MCB_1.0 (5.9 m^2 g^{-1}). These results are comparable with the figures of the previous study of silylated CNF aerogels (Zhang et al., 2014) but somewhat lower than CNF aerogels without silylation (Pääkkö et al., 2008). Moreover, the freeze-drying conditions, that is affected by e.g. thickness of the sample and cooling liquid, have substantial influence over nanofoam properties (Aulin et al., 2010; Macfarlane et al., 2012; Pääkkö et al., 2008).

The hierarchical microstructure of the nanofoam is formed during the freezing process in which the ice crystals tend to push the solid material to the interstitial regions of the crystals creating CNF-rich and CNF-sparse areas. Therefore, the morphology of nanofoams is strongly related to the growth and size of the ice crystals (Dash et al., 2012). Freeze drying of the nanofoams is used to preserve the microstructure formed during freezing process. Through reduction of the surrounding pressure, water sublimates directly from solid to gas phase, and the forces toward pore walls and structural damage occurring during drying are minimized (Rafieian et al., 2018). Fig. 6 presents the FESEM images

Fig. 5. Prepared nanofoams (MCB_0.3 on the left image and MCB_0.75 on the right) mounted in copper bush rings.
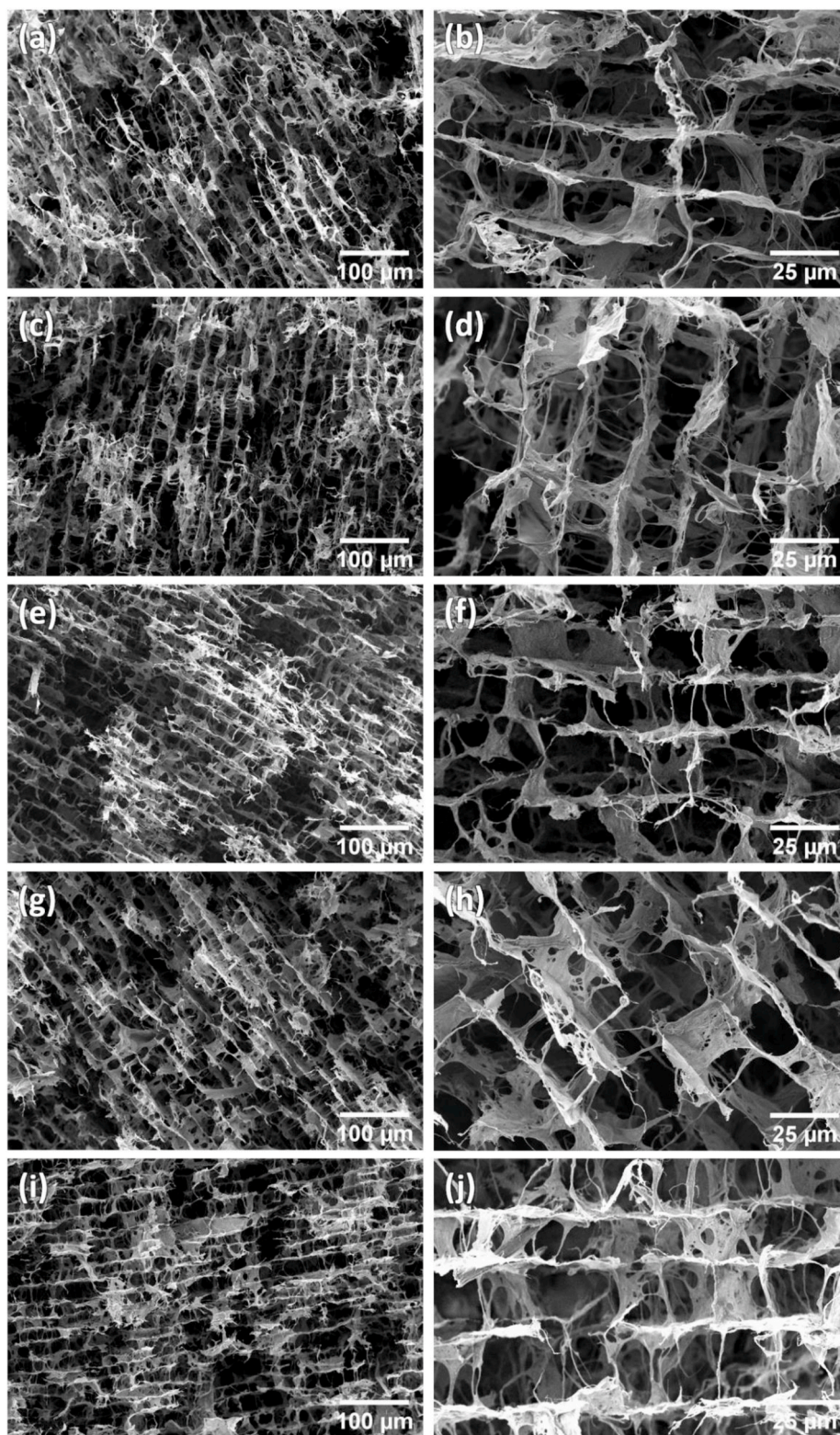
Fig. 6. FESEM images of the cross-sectional areas of the nanofoams prepared from various initial lignin-containing CNF concentrations: (a),(b) MCB_0.2%, (c),(d) MCB_0.3%, (e),(f) MCB_0.5%, (g),(h) MCB_0.75%, and (i),(j) MCB_1.0%. Images on the left side were obtained at 500 × magnification (scale bar = 100 μm), and the right-side magnification is 2000 × (scale bar = 25 μm).

of the nanofoams. The nanofibers are hydrogen bonded to each other and crosslinked with silanes to form a skeletal frame of an open-pore network where adjacent pores are separated by CNF layers and threads. The distance between layers is in the range of 15–25 μm. The apparent effect of higher CNF content is creation of broader and thicker cross-layer structures; by contrast, with lower CNF content, those structures and layers are thinner and minor. In accordance with FESEM images, nanofoams with lower CNF content have a more open structure and a slender frame that leads to a larger specific surface area.

Pore size distributions of similar MCB nanofoams had been earlier

studied using a set of advanced NMR techniques (Kharbanda et al., 2019) to determine the mean pore diameters of three characteristic pore size classes. The mean pore diameters of nanometer scale pores were close to 100 nm, and sub-millimeter pores were close to 200 μm. In these groups, there were only minor changes in mean diameters related to different CNF consistencies of nanofoams. The most distinct consistency-related differences to mean pore diameters were in prevalent micrometer scale pores. There, the mean pore diameter increased from 2.5 μm to 4.9 μm when nanofoam consistency decreased from 1.0% to 0.3%. The same difference is shown in Fig. 7 (a) and (b), where 0.3% and 1.0% nanofoams are compared. In both images, different pore size classes are visible; moreover, individual nanofibers, nanofiber aggregates, and threads can be noticed. A heterogeneous and hierarchical pore structure was hypothesized to have a good aerosol filtration performance due the complicated path each aerosol particle needs to take to penetrate the nanofoam. Moreover, varying dimensions of pores and solid material could enhance the probability of the particles with different sizes to be affected and intercepted on to the nanofoam structure and to result in wide particle capture distribution.

3.2. Filtration performance

Fig. 8 shows primary particle concentrations of NaCl from filtered (right, y-axis) and reference (left, y-axis) CPCs for 0.2–1.0 wt% MCB nanofoams (a, c, e, g, i) and corresponding filtration efficiencies (b, d, f, h, j). Average size distribution value obtained from three separate scans over the size distribution was used. 5 wt% NaCl solution resulted in high NaCl particle concentration, where the maximum concentration ($\sim$10,000 cm^{-3}) was obtained in the size range from $\sim$70 nm to $\sim$120 nm. The overall size distribution corresponded well to the atomizer-manufactured specifications.

In the current study the NaCl particles were dried in the diffusion dryer, which significantly reduces the potential effects of surface hydrophobicity on retention. The synthetic NaCl aerosols have a high purity surface, and their anionic surface charge is previously noted to change as a function of particle size (Forsyth et al., 1998). The retention of NaCl in the nanofoams is supposed to follow general mechanisms occurring during aerosol filtration and the retention mechanisms are generally size-dependent (Ding et al., 2019). Nanoscale particles (<100 nm) are efficiently filtered by Brownian diffusion (and electrostatic deposition if they are electrostatic materials) in nanofiber filters (Podgórski et al., 2006). In general, particles larger than 300 nm are filtered through interception and impaction mechanisms. This results in a minimum theoretical filtration efficiency with particles of around 100–300 nm (Barhate and Ramakrishna, 2007; Brown and Cox, 2017). In general, as the filter porosity (packing density, α) increases and the filter material's average fiber thickness d_F decreases, the fractional filtering efficiency rises along with the decrease in the most penetrating particle size (MPPS) (Podgórski et al., 2006). The NaCl concentration produced by the atomizer decreases exponentially after $\sim$200 nm. This causes some uncertainty in the large particle size range as the reference

signal drops and CPC noise remains constant. This could also cause variation in the collection efficiency in the 200–500 nm size range (Fig. 8).

Nanofibers with small diameters can be effective in removing submicron aerosols (Hung and Leung, 2011; Podgórski et al., 2006) as both diffusion and interception mechanisms are enhanced by the increase in the surface-to-volume ratio (Leung and Hung, 2012). On the contradictory, the pressure drop across the filter can be high (Macfarlane et al., 2012). The pressure drop (ΔP), filtering efficiency minima (Ef$_{min}$), and corresponding particle sizes (Ef$_{min}$, Dp), as well as quality factor values (QF$_{min}$, QF$_{min}$, Dp) across different studied filters are presented in Table 2. The pressure difference increased as the nanofiber content of nanofoams increased from 0.3 wt% to 1.0 wt%. However, the pressure difference of 0.2 wt% nanofoam was slightly higher than that of the 0.3 wt% sample. The 0.2 wt% nanofoam was very soft, and, presumably, the sample was compressed by the flow and packed more densely. Therefore, the 0.3 wt% nanofoam seemed to have the optimum structure in terms of pressure loss.

The lowest value in the filtering efficiency (96%) was obtained with the 0.2 wt% nanofoam at a 180 nm particle size. The nanofoams with the highest nanofiber content (0.75 wt% and 1.0 wt%) in turn displayed over 99.5% filtration efficiency at the particle size range from $\sim$26 to 360 nm and from $\sim$30 to 310 nm, respectively. In the literature, there are a few other studies regarding to aerosol filtration performance of cellulose nanofiber aerogels or similar materials. Macfarlane et al. (2012) used fibrillated wood pulp and anionic polyacrylamide to produce air filters achieving satisfactory performance and meeting NIOSH N95 standard for respirator face masks ("Approval of respiratory protective devices. In Code of Federal Regulations, Title 42 - Public Health, part 84.," n. d.) (filtration efficiency over 95% measured at the MPPS and pressure drop less than 250 Pa with a face velocity of $\sim$8.7 cm s^{-1}). The crucial challenge was to achieve simultaneously both the low-enough pressure drop and the high efficiency. Alexandrescu et al. (2016) prepared microfibrillated cellulose-based filters by freeze drying, yielding low pressure drop and low efficiency (55 Pa and 56%, 25 Pa and 46%). Lu et al. (2018) reported the preparation of the fibrillated cellulose-based air filters using tert-butyl alcohol in the freeze-drying process. By measuring filter efficiency at assumed MPPS (0.3 μm) high filtration efficiency with moderate pressure drop, 99.07%–99.78% and 100–400 Pa respectively, was achieved, indicating that the filtration efficiency met the N99 standard ("Approval of respiratory protective devices. In Code of Federal Regulations, Title 42 - Public Health, part 84.," n. d.).

Fig. 9 presents the quality factor (QF) of nanofoam filters calculated for the particle size range from 10 nm to 500 nm. QF value is independent of the thickness and porosity of the samples and can be used for quantitative evaluation of filter performance. The lowest pressure drop value was measured within the 0.3 wt% sample, for which the highest QF value was also obtained. For the rest of the nanofoams filters, the pressure drop increased with the CNF wt% resulting in lower QF values. In general, our filters suffered from the high induced pressure drop,
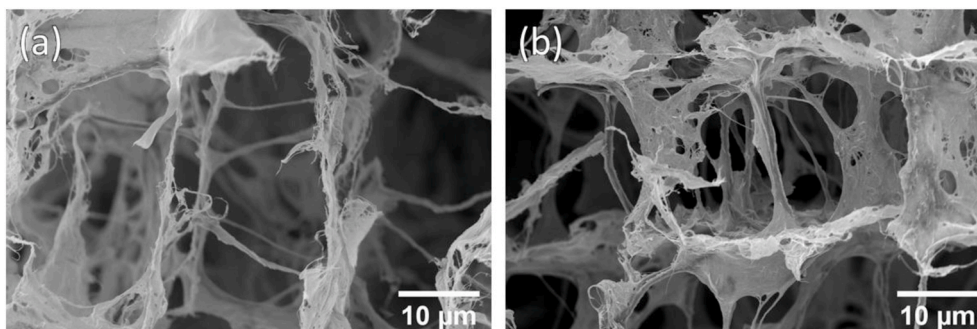

Fig. 7. Close-up FESEM images of (a) MCB_0.3% and (b) MCB_1.0% nanofoams with 5000 × magnification (scale bar = 10 μm).
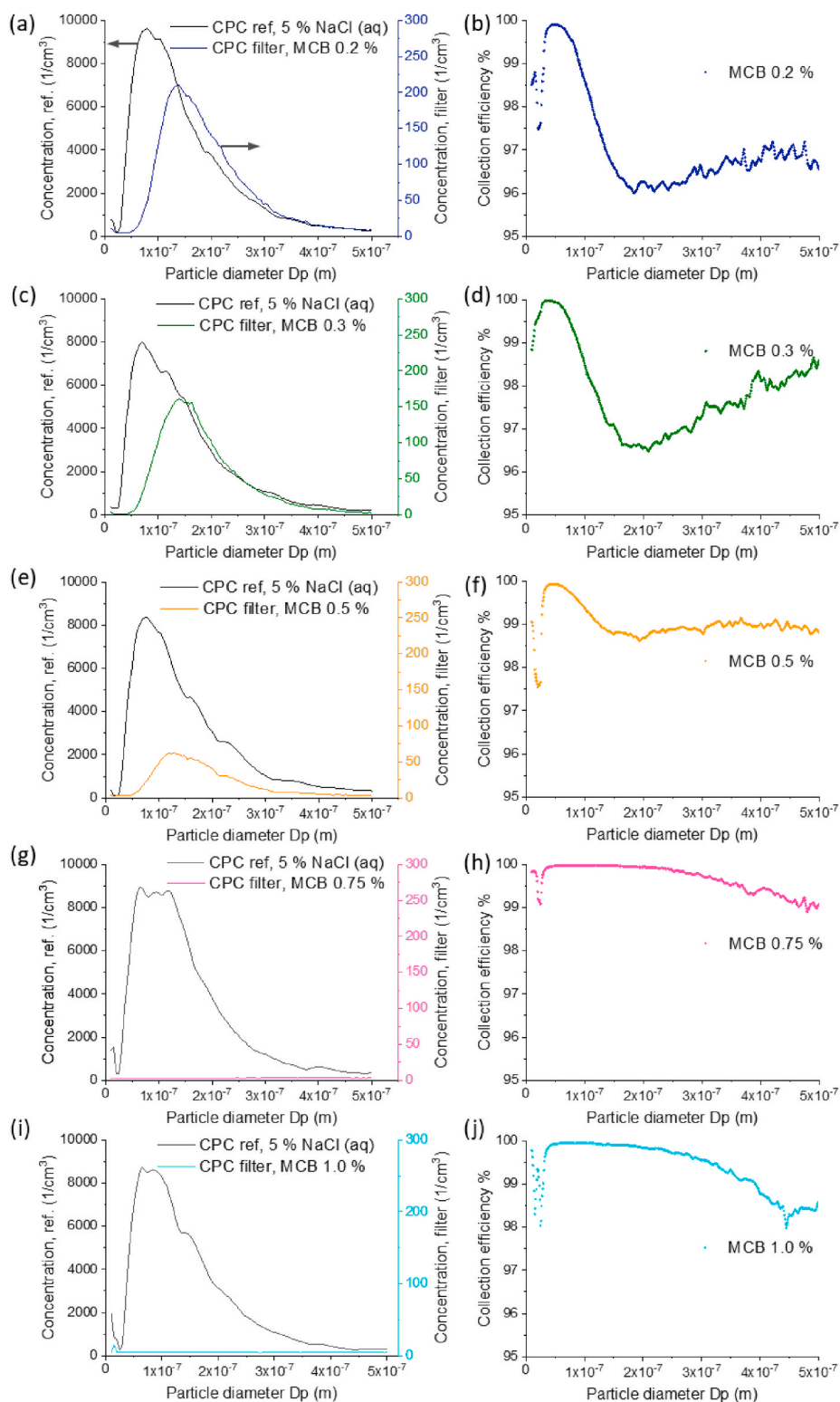
Fig. 8. NaCl particle distributions from filtered and reference CPCs for 0.2–1.0 wt% MCB nanofoams (a, c, e, g, i) and corresponding filtration efficiencies (b, d, f, h, j), respectively. Particle distributions and filtration efficiencies on each sample were averaged from three scans.

which was mainly caused by considerable thickness of the filters (12 mm), which was in turn set by the measurement instrumentation. Most of the nanofibrous filters reported have been typically harnessed in the form of thin membranes or mats (Gopal et al., 2006; Lu et al., 2018; Ma et al., 2018; Matulevicius et al., 2016) or thin-coated on a substrate filtering media (Leung et al., 2010; Nemoto et al, 2015, 2016). These types of filters are capable of capturing even the smallest aerosol

particles because of their nanofibrous character and small porosity. By contrast, particles accumulate on the surface of the filter leading decreased permeability and increased resistance of the flow. Deuber et al. (2018) prepared high-efficiency and ultralight nanofiber nanofoams with similar characteristics to those of our MCB nanofoams. These nanofoams could sustain very high particle loadings without loss in the filtration performance or increase in the flow resistance. In this regard,

Table 2
Differential pressures (filter pressure drop) for 0.2–1.0 wt% MCB nanofoam filter samples with the face velocity of 5.3 cm s^{-1} and particle diameter values (Dp) for most penetrating particle size obtained from QF values and filtering efficiency values (Ef).

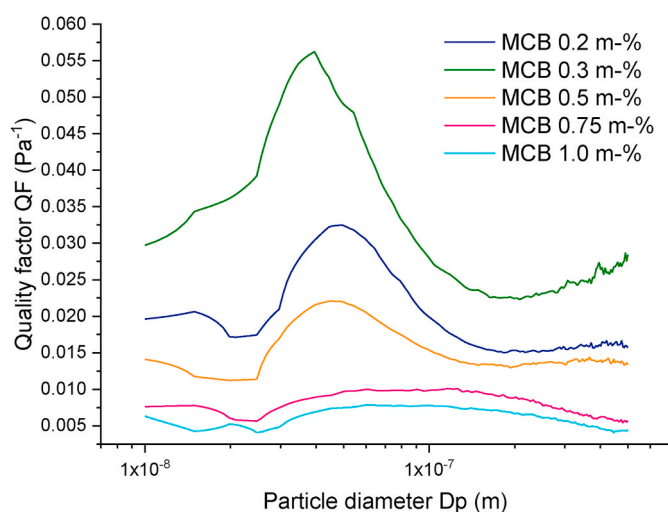| MCB (wt %)	ΔP (Pa)	ΔP (mbar)	Ef$_{min}$ (%)	Ef$_{min}$, Dp (m)	QF$_{min}$ (Pa^{-1})	QF$_{min}$, Dp (m)
0.2	214.4 ± 10.7	2.1 ± 0.1	96.0	1.8 × 10^{-7}	0.015	2.4 × 10^{-7}
0.3	150.0 ± 7.5	1.5 ± 0.1	96.5	2.1 × 10^{-7}	0.002	2.1 × 10^{-7}
0.5	330.0 ± 16.5	3.3 ± 0.2	97.5	2.0 × 10^{-7}	0.013	1.9 × 10^{-7}
0.75	830.0 ± 41.5	8.3 ± 0.4	98.9	4.8 × 10^{-7}	0.006	4.8 × 10^{-7}
1	958.9 ± 47.9	9.6 ± 0.5	98.0	4.5 × 10^{-7}	0.004	4.9 × 10^{-7}

Fig. 9. Quality factors for 0.2 wt%, 0.3 wt%, 0.5 wt%, 0.75 wt%, and 1.0 wt% MCB nanofoams as functions of NaCl particle diameter under the face velocity of 5.3 cm s^{-1}.

our filters can potentially improve the filter quality in terms of endurance and durability.

3.3. Evaluation of reliability of the filtration setup

Particle number size distribution for the size ranging from 20 nm to 200 nm determined by DMPS setups are in general within the uncertainty range of around ±10% (Wiedensohler et al., 2012). For the larger particles, the uncertainty increases due to lower counting statistics of the primary NaCl particle distribution produced by the atomizer. Thus, prior to the measurements, a PLS with a nominal diameter of 200 ± 5.3 nm was measured to validate the size calibration for the current setup (Fig. 4, right).

In the DMA, the NaCl particles are classified by their electrical mobility and, especially lower-size-range NaCl particles, are mainly single charged. It should be, however, noted that each size of the sample aerosol flow with given electrical mobility always contains some particles with different sizes and charges due to multiple charging phenomena (Wiedensohler, 1988). Changes in particle number concentration due to multiple charging can be corrected using upstream and downstream concentrations under bipolar charge distribution (Leung et al., 2010). This method might be useful when there are enough signals at given multiple charged sizes in C$_{filter}$. For example, a 500-nm-diameter double-charged particle would end up in the mobility size corresponding to a 295 nm diameter (Wiedensohler, 1988). However, the method

used by Leung et al. (2010) is not useful for high-efficiency filters, as there are no or very few larger (>200 nm) particles remaining for downstream CPC, as in the case of all current MCB samples.

4. Conclusions

In summary, crosslinked cellulose nanofiber nanofoams fabricated from recycled cellulose material are a potential high-efficiency filter material for aerosol filtration. The nanofoams consist of a biodegradable material that is readily disposed by, e.g., by incineration, and can potentially be used also for other purposes, such as indoor air purification and part of the face masks. The increase in CNF content of nanofoams yields better filtration efficiencies. In general, lignin-containing CNF nanofoams performed well within the 10–500 nm size range under the face velocity of 5.3 cm s^{-1}, achieving over 96% efficiency. Very high filtration efficiency (>99.5%) was achieved with the 0.7 wt% nanofoam sample for particle sizes ranging from 26 to 360 nm. Based on the quality factors, the 0.3 wt% nanofoam produced the lowest pressure drop yet with relatively high filtration efficiency and resulted in the highest QF value met the N95 standard requirements of respirator face masks. The structure of the thick nanofoam filter makes possible long-term filtration performance extending service or replacement interval.

Credit Author Statement

Jonne Ukkola participated in experimental design and conducted the major part of the experiments and prepared the first draft of the manuscript together with Markus Lampimäki. Markus Lampimäki, Tomi Vainio, Erkki Siivola and Ossi Laitinen conducted also part of the experimental work (filtration experiments; ML, TV, ES, preparation and analysis of nanofoams, OL). Henrikki Liimatainen, Ossi Laitinen, Tuukka Petäjä and Juha Kangasluoma participated in experimental design, supervision of the experimental work and writing and finalization of the manuscript.

Declaration of competing interest

The authors declare that they have no known competing financial interests or personal relationships that could have appeared to influence the work reported in this paper.

References

Ahn, Y.C., Park, S.K., Kim, G.T., Hwang, Y.J., Lee, C.G., Shin, H.S., Lee, J.K., 2006. Development of high efficiency nanofilters made of nanofibers. Curr. Appl. Phys., Nano Korea 2004 Symposium on NT Challenge 6, 1030–1035. https://doi.org/10.1016/j.cap.2005.07.013.

Alexandrescu, L., Syverud, K., Nicosia, A., Santachiara, G., Fabrizi, A., Belosi, F., 2016. Airborne nanoparticles filtration by means of cellulose nanofibril based materials. J. Biomaterials Nanobiotechnol. 7, 29–36. https://doi.org/10.4236/jbnb.2016.71004.

Aulin, C., Netrval, J., Wågberg, L., Lindström, T., 2010. Aerogels from nanofibrillated cellulose with tunable oleophobicity. Soft Matter 6, 3298–3305. https://doi.org/10.1039/C001939A.

Barhate, R.S., Ramakrishna, S., 2007. Nanofibrous filtering media: filtration problems and solutions from tiny materials. J. Membr. Sci. 296, 1–8. https://doi.org/10.1016/j.memsci.2007.03.038.

Front-matter. In: Brown, P.J., Cox, C.L. (Eds.), 2017. Fibrous Filter Media, Woodhead Publishing Series in Textiles. Woodhead Publishing. https://doi.org/10.1016/B978-0-08-100573-6.00013-7.

Dash, R., Li, Y., Ragauskas, A.J., 2012. Cellulose nanowhisker foams by freeze casting. Carbohydr. Polym. 88, 789–792. https://doi.org/10.1016/j.carbpol.2011.12.035.

Davidson, C.I., Phalen, R.F., Solomon, P.A., 2005. Airborne particulate matter and human health: a review. Aerosol Sci. Technol. 39, 737–749. https://doi.org/10.1080/02786820500191348.

Deuber, F., Mousavi, S., Federer, L., Hofer, M., Adlhart, C., 2018. Exploration of ultralight nanofiber aerogels as particle filters: capacity and efficiency. ACS Appl. Mater. Interfaces 10, 9069–9076. https://doi.org/10.1021/acsami.8b00455.

Ding, B., Wang, X., Yu, J., 2019. Electrospinning Nanofabrication and Applications. Elsevier., Amsterdam, p. 806. https://doi.org/10.1016/C2016-0-01374-8.

Fan, P., Yuan, Y., Ren, J., Yuan, B., He, Q., Xia, G., Chen, F., Song, R., 2017. Facile and green fabrication of cellulosed based aerogels for lampblack filtration from waste newspaper. Carbohydr. Polym. 162, 108–114. https://doi.org/10.1016/j.carbpol.2017.01.015.

Forsyth, B., Liu, B.Y.H., Romay, F.J., 1998. Particle charge distribution measurement for commonly generated laboratory aerosols. Aerosol Sci. Technol. 28, 489–501. https://doi.org/10.1080/02786829808965540.

Gopal, R., Kaur, S., Ma, Z., Chan, C., Ramakrishna, S., Matsuura, T., 2006. Electrospun nanofibrous filtration membrane. J. Membr. Sci. 281, 581–586. https://doi.org/10.1016/j.memsci.2006.04.026.

Huber, L., Zhao, S., Malfait, W.J., Vares, S., Koebel, M.M., 2017. Fast and minimal-solvent production of superinsulating silica aerogel granulate. Angew. Chem. Int. Ed. 56, 4753–4756. https://doi.org/10.1002/anie.201700836.

Hung, C.-H., Leung, W.W.-F., 2011. Filtration of nano-aerosol using nanofiber filter under low Peclet number and transitional flow regime. Separ. Purif. Technol. 79, 34–42. https://doi.org/10.1016/j.seppur.2011.03.008.

Innerlohinger, J., Weber, H.K., Kraft, G., 2006. Aerocellulose: aerogels and aerogel-like materials made from cellulose. Macromol. Symp. 244, 126–135. https://doi.org/10.1002/masy.200651212.

Jiang, F., Hsieh, Y.-L., 2014. Amphiphilic superabsorbent cellulose nanofibril aerogels. J. Mater. Chem. 2, 6337–6342. https://doi.org/10.1039/C4TA00743C.

Jin, H., Nishiyama, Y., Wada, M., Kuga, S., 2004. Nanofibrillar cellulose aerogels. Colloids Surf. Physicochem. Eng. Asp. 240, 63–67. https://doi.org/10.1016/j.colsurfa.2004.03.007.

Karzar Jeddi, M., Laitinen, O., Liimatainen, H., 2019. Magnetic superabsorbents based on nanocellulose aerobeads for selective removal of oils and organic solvents. Mater. Des. 183, 108115. https://doi.org/10.1016/j.matdes.2019.108115.

Katz, S., Beatson, R.P., Scallan, A.M., 1984. The determination of strong and weak acidic groups in sulfite pulps. Sven. Papperstidning 87, R48–R53.

Kharbanda, Y., Urbańczyk, M., Laitinen, O., Kling, K., Pallaspuro, S., Komulainen, S., Liimatainen, H., Telkki, V.-V., 2019. Comprehensive NMR analysis of pore structures in superabsorbing cellulose nanofiber aerogels. J. Phys. Chem. C 123, 30986–30995. https://doi.org/10.1021/acs.jpcc.9b08339.

Kim, K.-H., Kabir, E., Kabir, S., 2015. A review on the human health impact of airborne particulate matter. Environ. Int. 74, 136–143. https://doi.org/10.1016/j.envint.2014.10.005.

Kim, S.J., Chase, G., Jana, S.C., 2016. The role of mesopores in achieving high efficiency airborne nanoparticle filtration using aerogel monoliths. Separ. Purif. Technol. 166, 48–54. https://doi.org/10.1016/j.seppur.2016.04.017.

Kim, S.J., Raut, P., Jana, S.C., Chase, G., 2017. Electrostatically active polymer hybrid aerogels for airborne nanoparticle filtration. ACS Appl. Mater. Interfaces 9, 6401–6410. https://doi.org/10.1021/acsami.6b14784.

Korhonen, J.T., Kettunen, M., Ras, R.H.A., Ikkala, O., 2011. Hydrophobic nanocellulose aerogels as floating, sustainable, reusable, and recyclable oil absorbents. ACS Appl. Mater. Interfaces 3, 1813–1816. https://doi.org/10.1021/am200475b.

Kulmala, M., Petäjä, T., Nieminen, T., Sipilä, M., Manninen, H.E., Lehtipalo, K., Dal Maso, M., Aalto, P.P., Junninen, H., Paasonen, P., Riipinen, I., Lehtinen, K.E.J., Laaksonen, A., Kerminen, V.-M., 2012. Measurement of the nucleation of atmospheric aerosol particles. Nat. Protoc. 7, 1651–1667. https://doi.org/10.1038/nprot.2012.091.

Laitinen, O., Suopajärvi, T., Österberg, M., Liimatainen, H., 2017. Hydrophobic, superabsorbing aerogels from choline chloride-based deep eutectic solvent pretreated and silylated cellulose nanofibrils for selective oil removal. ACS Appl. Mater. Interfaces 9, 25029–25037. https://doi.org/10.1021/acsami.7b06304.

Leung, W.W.-F., Hung, C.-H., 2012. Skin effect in nanofiber filtration of submicron aerosols. Sep. Purif. Technol., Papers presented at European Conference on Fluid-Particle Separation (FPS 2010) 92, 174–180. https://doi.org/10.1016/j.seppur.2011.02.020.

Leung, W.W.-F., Hung, C.-H., Yuen, P.-T., 2010. Effect of face velocity, nanofiber packing density and thickness on filtration performance of filters with nanofibers coated on a substrate. Separ. Purif. Technol. 71, 30–37. https://doi.org/10.1016/j.seppur.2009.10.017.

Lu, T., Li, Q., Chen, W., Yu, H., 2014. Composite aerogels based on dialdehyde nanocellulose and collagen for potential applications as wound dressing and tissue engineering scaffold. Compos. Sci. Technol. 94, 132–138. https://doi.org/10.1016/j.compscitech.2014.01.020.

Lu, Z., Su, Z., Song, S., Zhao, Y., Ma, S., Zhang, M., 2018. Toward high-performance fibrillated cellulose-based air filter via constructing spider-web-like structure with the aid of TBA during freeze-drying process. Cellulose 25, 619–629. https://doi.org/10.1007/s10570-017-1561-x.

Ma, S., Zhang, M., Yang, B., Song, S., Nie, J., Lu, P., 2018. Preparation of cellulosic air filters with controllable pore structures via organic solvent-based freeze casting: the key role of fiber dispersion and pore size. BioResources 13, 5894–5908.

Ma, X.Y.D., Ang, J.M., Zhang, Y., Zeng, Z., Zhao, C., Chen, F., Ng, B.F., Wan, M.P., Wong, S.-C., Li, Z., He, C., Lu, X., 2019. Highly porous polymer nanofibrous aerogels cross-linked via spontaneous inter-fiber stereocomplexation and their potential for capturing ultrafine airborne particles. Polymer 179, 121649. https://doi.org/10.1016/j.polymer.2019.121649.

Macfarlane, A.L., Kadla, J.F., Kerekes, R.J., 2012. High performance air filters produced from freeze-dried fibrillated wood pulp: fiber network compression due to the freezing process. Ind. Eng. Chem. Res. 51, 10702–10711. https://doi.org/10.1021/ie301340q.

Maciej, Strak, Janssen Nicole, A.H., Godri Krystal, J., Gosens Ilse, Mudway Ian, S., Cassee Flemming, R., Erik, Lebret, Kelly Frank, J., Harrison Roy, M., Bert, Brunekreef, Maaike, Steenhof, Hoek, Gerard, 2012. Respiratory health effects of airborne particulate matter: the role of particle size, composition, and oxidative potential—the RAPTES project. Environ. Health Perspect. 120, 1183–1189. https://doi.org/10.1289/ehp.1104389.

Mader, M., Jérôme, V., Freitag, R., Agarwal, S., Greiner, A., 2018. Ultraporous, compressible, wettable polylactide/polycaprolactone sponges for tissue engineering. Biomacromolecules 19, 1663–1673. https://doi.org/10.1021/acs.biomac.8b00434.

Matulevicius, J., Kliucininkas, L., Prasauskas, T., Buivydiene, D., Martuzevicius, D., 2016. The comparative study of aerosol filtration by electrospun polyamide, polyvinyl acetate, polyacrylonitrile and cellulose acetate nanofiber media. J. Aerosol Sci. 92, 27–37. https://doi.org/10.1016/j.jaerosci.2015.10.006.

Nechyporchuk, O., Belgacem, M.N., Bras, J., 2016. Production of cellulose nanofibrils: a review of recent advances. Ind. Crops Prod., Nanocellulose: production, functionalisation and applications 93, 2–25. https://doi.org/10.1016/j.indcrop.2016.02.016.

Nemoto, J., Saito, T., Isogai, A., 2015. Simple freeze-drying procedure for producing nanocellulose aerogel-containing, high-performance air filters. ACS Appl. Mater. Interfaces 7. https://doi.org/10.1021/acsami.5b05841, 19809–19815.

Nemoto, J., Soyama, T., Saito, T., Isogai, A., 2016. Improvement of air filters by nanocelluloses. 紙パ技協誌 70, 1072–1078. https://doi.org/10.2524/jtappi.70.1072.

Nissilä, T., Hietala, M., Oksman, K., 2019. A method for preparing epoxy-cellulose nanofiber composites with an oriented structure. Compos. Part Appl. Sci. Manuf. 125, 105515. https://doi.org/10.1016/j.compositesa.2019.105515.

Pääkkö, M., Vapaavuori, J., Silvennoinen, R., Kosonen, H., Ankerfors, M., Lindström, T., Berglund, L.A., Ikkala, O., 2008. Long and entangled native cellulose I nanofibers allow flexible aerogels and hierarchically porous templates for functionalities. Soft Matter 4, 2492–2499. https://doi.org/10.1039/B810371B.

Park, K., Kim, J.-S., Miller, A.L., 2009. A study on effects of size and structure on hygroscopicity of nanoparticles using a tandem differential mobility analyzer and TEM. J. Nanoparticle Res. 11, 175–183. https://doi.org/10.1007/s11051-008-9462-4.

Podgórski, A., Bałazy, A., Gradoń, L., 2006. Application of nanofibers to improve the filtration efficiency of the most penetrating aerosol particles in fibrous filters. Chem. Eng. Sci. 61, 6804–6815. https://doi.org/10.1016/j.ces.2006.07.022.

Qian, Z., Wang, Z., Chen, Y., Tong, S., Ge, M., Zhao, N., Xu, J., 2018. Superelastic and ultralight polyimide aerogels as thermal insulators and particulate air filters. J. Mater. Chem. 6, 828–832. https://doi.org/10.1039/C7TA09054D.

Qiao, S., Zhang, H., Kang, S., Quan, J., Hu, Z., Yu, J., Wang, Y., Zhu, J., 2020. Hydrophobic, pore-tunable polyimide/polyvinylidene fluoride composite aerogels for effective airborne particle filtration. Macromol. Mater. Eng. 305, 2000129. https://doi.org/10.1002/mame.202000129.

Rafieian, F., Hosseini, M., Jonoobi, M., Yu, Q., 2018. Development of hydrophobic nanocellulose-based aerogel via chemical vapor deposition for oil separation for water treatment. Cellulose 25, 4695–4710. https://doi.org/10.1007/s10570-018-1867-3.

Rattaz, A., Mishra, S.P., Chabot, B., Daneault, C., 2011. Cellulose nanofibres by sonocatalysed-TEMPO-oxidation. Cellulose 18, 585–593. https://doi.org/10.1007/s10570-011-9529-8.

Sehaqui, H., Salajková, M., Zhou, Q., Berglund, L.A., 2010. Mechanical performance tailoring of tough ultra-high porosity foams prepared from cellulose I nanofiber suspensions. Soft Matter 6, 1824–1832. https://doi.org/10.1039/B927505C.

Shah, A.S., Langrish, J.P., Nair, H., McAllister, D.A., Hunter, A.L., Donaldson, K., Newby, D.E., Mills, N.L., 2013. Global association of air pollution and heart failure: a systematic review and meta-analysis. Lancet 382, 1039–1048. https://doi.org/10.1016/S0140-6736(13)60898-3.

Siegel, J.D., Rhinehart, E., Jackson, M., Chiarello, L., 2007. 2007 guideline for isolation precautions: preventing transmission of infectious agents in health care settings. Am. J. Infect. Contr. 35, S65–S164. https://doi.org/10.1016/j.ajic.2007.10.007.

Souzandeh, H., Wang, Y., Netravali, A.N., Zhong, W.-H., 2019. Towards sustainable and multifunctional air-filters: a review on biopolymer-based filtration materials. Polym. Rev. 59, 651–686. https://doi.org/10.1080/15583724.2019.1599391.

Subbiah, T., Bhat, G.S., Tock, R.W., Parameswaran, S., Ramkumar, S.S., 2005. Electrospinning of nanofibers. J. Appl. Polym. Sci. 96, 557–569. https://doi.org/10.1002/app.21481.

Suopajärvi, T., Sirviö, J.A., Liimatainen, H., 2017. Nanofibrillation of deep eutectic solvent-treated paper and board cellulose pulps. Carbohydr. Polym. 169, 167–175. https://doi.org/10.1016/j.carbpol.2017.04.009.

Tsai, P.P., Schreuder-Gibson, H., Gibson, P., 2002. Different electrostatic methods for making electret filters. J. Electrost., Selected Papers from the 28th Annual Conference of the Electrosta tics Society of America 54, 333–341. https://doi.org/10.1016/S0304-3886(01)00160-7.

Wang, W., Fang, Y., Ni, X., Wu, K., Wang, Y., Jiang, F., Riffat, S.B., 2019. Fabrication and characterization of a novel konjac glucomannan-based air filtration aerogels strengthened by wheat straw and okara. Carbohydr. Polym. 224, 115129. https://doi.org/10.1016/j.carbpol.2019.115129.

Wang, D., Peng, H., Yu, B., Zhou, K., Pan, H., Zhang, L., Li, M., Liu, M., Tian, A., Fu, S., 2020. Biomimetic structural cellulose nanofiber aerogels with exceptional mechanical, flame-retardant and thermal-insulating properties. Chem. Eng. J. 389, 124449. https://doi.org/10.1016/j.cej.2020.124449.

Wiedensohler, A., 1988. An approximation of the bipolar charge distribution for particles in the submicron size range. J. Aerosol Sci. 19, 387–389. https://doi.org/10.1016/0021-8502(88)90278-9.

Wiedensohler, A., Birmili, W., Nowak, A., Sonntag, A., Weinhold, K., , Merkel, M., Wehner, B., Tuch, T., Pfeifer, S., Fiebig, M., Fjäraa, A.M., Asmi, E., Sellegri, K., Depuy, R., Venzac, H., Villani, P., Laj, P., Aalto, P., Ogren, J.A., Swietlicki, E., Williams, P., Roldin, P., Quincey, P., Hüglin, C., Fierz-Schmidhauser, R., Gysel, M., Weingartner, E., Riccobono, F., Santos, S., Grüning, C., Faloon, K., Beddows, D., Harrison, R., Monahan, C., Jennings, S.G., O'Dowd, C.D., Marinoni, A., Horn, H.-G., Keck, L., Jiang, J., Scheckman, J., McMurry, P.H., Deng, Z., Zhao, C.S., Moerman, M., Henzing, B., Leeuw, G. de, Löschau, G., Bastian, S., 2012. Mobility particle size spectrometers: harmonization of technical standards and data structure to facilitate high quality long-term observations of atmospheric particle number size distributions. Atmospheric Meas. Tech. 5, 657–685. https://doi.org/10.5194/amt-5-657-2012.

Wu, J., Zeng, L., Huang, X., Zhao, L., Huang, G., 2017. Mechanically robust and shape-memory hybrid aerogels for super-insulating applications. J. Mater. Chem. 5, 15048–15055. https://doi.org/10.1039/C7TA02686B.

Zanini, M., Lavoratti, A., Lazzari, L.K., Galiotto, D., Pagnocelli, M., Baldasso, C., Zattera, A.J., 2017. Producing aerogels from silanized cellulose nanofiber suspension. Cellulose 24, 769–779. https://doi.org/10.1007/s10570-016-1142-4.

Zeng, Z., Ma, X.Y.D., Zhang, Y., Wang, Z., Ng, B.F., Wan, M.P., Lu, X., 2019. Robust lignin-based aerogel filters: high-efficiency capture of ultrafine airborne particulates and the mechanism. ACS Sustain. Chem. Eng. 7, 6959–6968. https://doi.org/10.1021/acssuschemeng.8b06567.

Zhai, C., Jana, S.C., 2017. Tuning porous networks in polyimide aerogels for airborne nanoparticle filtration. ACS Appl. Mater. Interfaces 9, 30074–30082. https://doi.org/10.1021/acsami.7b09345.

Zhang, Z., Sèbe, G., Rentsch, D., Zimmermann, T., Tingaut, P., 2014. Ultralightweight and flexible silylated nanocellulose sponges for the selective removal of oil from water. Chem. Mater. 26, 2659–2668. https://doi.org/10.1021/cm5004164.

Zhang, Z., Tingaut, P., Rentsch, D., Zimmermann, T., Sèbe, G., 2015. Controlled silylation of nanofibrillated cellulose in water: reinforcement of a model polydimethylsiloxane network. ChemSusChem 8, 2681–2690. https://doi.org/10.1002/cssc.201500525.

Zhang, S., Sun, J., Hu, D., Xiao, C., Zhuo, Q., Wang, J., Qin, C., Dai, L., 2018. Large-sized graphene oxide/modified tourmaline nanoparticle aerogel with stable honeycomb-like structure for high-efficiency $PM_{2.5}$ capture. J. Mater. Chem. 6, 16139–16148. https://doi.org/10.1039/C8TA05506H.

Zhang, Y., Zeng, Z., Ma, X.Y.D., Zhao, C., Ang, J.M., Ng, B.F., Wan, M.P., Wong, S.-C., Wang, Z., Lu, X., 2019. Mussel-inspired approach to cross-linked functional 3D nanofibrous aerogels for energy-efficient filtration of ultrafine airborne particles. Appl. Surf. Sci. 479, 700–708. https://doi.org/10.1016/j.apsusc.2019.02.173.